International Journal of Advanced Engineering Research and Science (IJAERS)
Peer-Reviewed Journal
ISSN: 2349-6495(P) | 2456-1908(O)
Vol-8, Issue-12; Dec, 2021
Journal Home Page Available: https://ijaers.com/
Article DOI: https://dx.doi.org/10.22161/ijaers.812.29

Low Inrıdıum-Doped TiO_2 Nanostructure for Promısıng Photocatalyst ın Hexane Treatment

Van Thi Thanh Ho[1,*], Ngan Thi Thanh Nguyen[1], Dung Hung Chau[1], Nhat Minh Nguyen[1], Khang Quang Bui[2], Long Tran Hoang Nguyen[2], Khang Huy Le[2], Son Nguyen Truong[2]

[1]Hochiminh City University of Natural Resources and Environment (HCMUNRE), Vietnam

[2]Ho Chi Minh City University of Technology, VNU-HCM

[*]Corresponding author' e-mail: httvan@hcmunre.edu.vn

Received: 01 Nov 2021,

Received in revised form: 08 Dec 2021,

Accepted: 15 Dec 2021,

Available online: 26 Dec 2021

***Keywords*— photocatalysts, M-doped TiO_2, VOCs, n-hexane**

Abstract *— M-doped TiO_2 (with M: noble metal) photocatalysts are being extensively applied for volatile organic compounds (VOCs) treatment because of their wide range of gaseous VOCs treating ability and their lower cost in comparison to other methods. However, the efficiency in removing volatile gaseous VOCs of M-doped TiO_2 photocatalysts is relatively low due to the insufficient decrease of the band gap after doping (E_g < 3.0 eV), relatively low surface area (< 100 m^2/g) for using sol-gel method in combination with thermal treating at high temperature (>500 °C). In this work, we have solved current issues of TiO_2 photocatalysts by synthesizing nano-scaled advanced-structured Ir-doped TiO_2 materials in photocatalyst application for n-hexane decomposition, which has not been studied lately. The Ir-doped TiO_2 photocatalyst is synthesized by one-stage hydrothermal method without using any surfactant or heating process after reactions. We found that the efficiency in n-hexane treatment of Ir-doped TiO_2 photocatalyst with different ratios is relatively higher than other previous studies. It can be explained by the synthesis process of Ir-doped TiO_2 material optimizing nano-scaled particles (10-15mm), large surface area (170 m^2/g) and good crystallinity with the combination of anatase phase and rutile phase. Specially, Ir doping reduces the band gap of Ir-doped TiO_2 material from 2.5 to 2.7 eV, compared to 3.2eV of undoped -TiO_2 material's band gap, depending on the doping ratio in which the function of doped Ir metal is affecting the*

activity in photoreaction of TiO_2 by electrons or holes "traping" mechanism changing the electron/hole combination rate, hence enhancing the n-hexane treating efficiency.

I. INTRODUCTION

Recently, photocatalysts are becoming promisingly alternative material for air treatment due to some advantages such as the ability to deal with wide range of pollutants, high efficiency, simple operation and maintenance, reducing energy needed for degradation of volatile organic compounds (VOCs), therefore they can improve the quality of the air [1-3]. However, the application of TiO_2 photocatalyst material is still limited because of the short range of wavelength affected ($\lambda < 400nm$) and the low adsorption capacity of solar and indoor raditions (less than 5%) because the band gap of TiO_2 has relatively high energy (anatase TiO_2, ~3.2 eV) [5-6]. To solve this issue, some methods of enhacing efficiency of TiO_2 photocatalyst have been studied. In those methods, the method of doping metals into TiO_2 lattice structure is considered as the sufficient approach to narrow the band gap [7-8] and decline the rate of recombination of electrons and holes, thus improve the photocatalytical efficiency of TiO_2 in visible light region [9]. In 2011, *Ming Jin et al.* [12] synthesized the W-doped TiO_2 photocatalyst by electrospining method and heating at 550^0C to decompose acetone. The result showed that W-doped TiO_2 photocatalyst has the high capacity of acetone oxidation. It can be explained by the reduction mechanism from W^{6+} to W^{5+}, in which W^{6+} donates the photogenic electrons to prevent the recombination of electron-hole pair. However, by experimenting different of W/Ti ratios, from 2% to 8%, the authors concluded that with the increased proportion of W doped, the photocatalytic activity decreased. *M. Hinojosa-Reyes* et al. (2013) [13] used the perlite granules coated with In-doped TiO_2 photocatalyst to decompose ethylbenzene gas [13]. The In-doped TiO_2 materials, containing 1.0 and 5.0 wt% of In doped, are synthesized by sol-gel method from Titanium (IV) isopropoxide and Inidium (III) acetylacetonate precusors, then heated at $400\ ^\circ C$ in 4 hours. The products showed that 5.0 wt% In-doped TiO_2/perlite photocatalyst has the ehtylbenzene degradation efficiency of ~25% in 40 minutes, higher than the efficiencies of TiO_2 (P25) photocatalyst with ~15%. However, the result also showed that 5 wt% In-doped TiO_2 photocatalyst has the band gap of 3.32 eV, which is higher than the band gap of commercial TiO_2 (P25) photocatalyst (3.26 eV). This is also the limit of the In-doped TiO_2 photocatalyst in visible light region.

In 2014, *Siva Nagi ReddyInturi* et al. [14] also investigated a series of M-doped TiO_2 photocatalyst materials (M = V, Cr, Fe, Co, Mn, Mo, Ni, Cu, Y, Ce, and Zr) to decompose acetonitrile vapor. The M-doped TiO_2 photocatalyst material was synthesized by the method of Flame Spray Pyrolysis (FSP). Within the investigated M-doped TiO_2 photocatalysts, the Cr-doped TiO_2 photocatalysts presented outstanding activity with the energy bandgap, which reduced to 2.90 eV under visible irradiation. At the same time, M-doped samples of other metals do not have similar activity in the identical experimental condition. The superior activity of Cr-doped TiO_2 was explained by the migration of electrons from TiO_2 to the Cr component, leading to a strong Cr-O-Ti bond. After investigating M-doped activities under visible radiation, the author concluded that the photolysis activity of the Cr-doped TiO_2 sample performed 8 to 19 times higher than others, ranking then were Fe and V doped samples, and other metals had negligible activity, respectively. In 2015, Haibao Huang et al. [15] investigated a series of transition metals (Mn, Co, Cu, Ni, Fe) doping into the TiO_2 network to improve the benzene

decomposition under vacuum ultraviolet (VUV) irradiation. M-doped TiO_2 photocatalysts (M = Mn, Co, Cu, Ni, Fe) were synthesized by the sol-gel method and calcined at $550\ °C$ C for 4 hours. The particle size range of the resulting photocatalyst material has about 10-40 nm, and the specific surface area is < 50 m^2/g. The results show that the Mn-doped TiO_2 material has the highest benzene decomposition efficiency (~58.0%) and ozone in the range of investigated materials. However, previous work has only focused on the treatment of acetone [10, 12], ethylbenzene [13], xylene [11]; few researchers have addressed the problems of the n-hexane organic compounds treatment. The treatment efficiency of n-hexane treated by M-doped TiO_2 photocatalyst was shallow because the M-doped TiO_2 photocatalyst materials still give bandgap energy > 3.0 eV [16, 17]. In addition, the sol-gel method combined with the post-reaction calcination stage were often used to synthesize M-doped TiO_2 photocatalysts, resulting in large particle size and low specific surface area (<100 m^2/g) [15, 16, 18] should lead to low decomposition efficiency of volatile organic compounds (VOCs). LexuanZhong et al., 2013 [4] studied how to coat TiO_2 particles on glass fibers by coating the support; the results were obtained TiO_2 particles with particle size about 3.5 nm and decomposed n-hexane with n-hexane concentration: 500 ppb, relative humidity: 40-60%. The resulting yield was 25%.

In this study, we want to solve the above problems of M-doped TiO_2 photocatalyst by synthesizing the new nanostructure of Ir-doped TiO_2 with low and different Iridium concentrations which is applied as photocatalyst for n-hexane decomposing which has not been studied before [19-21]. By doping metallic Ir into TiO_2 structure, the band gap can be reduced by more than 25% compared to the band gap of undoped-TiO_2 photocatalysts [22] due to the approximation in the radius of Ir^{4+} ion (r_{Ir} = 0.625 Å) and Ti^{4+} ion (r_{Ti} = 0.605 Å) increases the efficiency in doping Ir compared to doping other elements, thus it reduces the band gap of TiO_2 significantly. Furthermore, Iridium has some unique properties such as anti-sintering, lower surface coverage, charge spray properties, and non-toxicity, which cannot be found in other metals [21, 23-25, 26] so that it could be improved the n-hexane decomposition efficiency.

II. EXPERIMENTS

2.1 Synthesis of Ir-doped TiO_2 Photocatalyst

The Ir-doped TiO_2 photocatalyst is synthesized by single-stage hydrothermal method at low-temperature without using of any surfactant or stabilizers or post-reaction heat treatment. First, a quantity of salt (0.0035g; 0.0070g; 0.0105g, respectively correspond to 0.5%, 1.0% and 1.5% of Ir) $IrCl_3.xH_2O$ was dissolved in 50 ml of distilled water. Because TiCl4 is easily hydrolyzed at room temperature, so it is necessary to adjust pH = 1.5 to limit the hydrolysis of TiCl4. Using micropipet add 220µL $TiCl_4$ into solution. The solution sample was transferred to the autoclave at 210 °C and in 8 hours. After the end of the reaction time, the solution was allowed to cool naturally in air at room temperature, then centrifuged, filtered for solids and washed several times with distilled water until the pH reached neutral. Finally, the precipitate was dried at 80oC for 8 hours to obtain Ir-doped TiO_2 photocatalyst.

2.2 Material Characterization

The crystal structure analysis of the obtained samples was analyzed using a Bruker D8 Advance X-ray diffractometer using Cu K_α radiation (λ = 1.540598 nm) in the 2θ range of $10 - 80\ °$ at a scanning rate (2θ) of 5 min^{-1}. The morphologies of the pure TiO_2 and Ir-doped TiO_2 samples were characterized by field emission scanning electron microscopy (SEM) on a HitachiS-4800, transmission electron microscopy (TEM) on a JEM 1400 operated at 100 kV and field-emission high-resolution transmission electron microscopy

(HRTEM) on a TALOS F200x with an acceleration voltage of 200 kV equipped with an energy-dispersive X-ray spectroscopic analysis (EDS) system. X-ray fluorescence (XRF) measurement was performed on ARL ADVANT'X (Thermo) at an accelerating voltage of 30 kV to record the elemental composition in the as-obtained nanomaterials. In the BET method, N_2 adsorption/desorption isotherms were performed on NOVA 1000e at 77K to measure the surface area and pore size of the TixIr1-xO2 catalysts. Before BET measurements, the specimens were degassed/dried at $250\ °C$ for 3 hours to eliminate water molecules adsorbed in the meso/micropores of the catalyst support. Measurements of the UV-visible diffuse reflectance spectra (DRS) of samples were carried out on a UV-Vis spectrophotometer (JASCO-V670) at room temperature in the range of 350−800 nm.

2.3 N-hexane treatment System

n-hexane (C_6H_{12}) oxidation reactions occuring on the new nano-scaled Ir-doped TiO_2 photocatalyst are performed in a specifically built system. The concentration of gas n-hexane is measured before and after being blown through the photocatalyst for analysing photocatalytic properties of the material.

The experimental system is shown in Figuer 1 includes:

- A P1 pump blowing air into the system
- A glassy column containing silicagel material, which is kept by two rubber caps and glassy cotton to remove humidity out of inlet air.
- A glassy column containing activated carbon to clean and remove the residual humidity.
- A F1 flowmeter to control the air flow rate.
- A 5mm – diameter glassy tube containing a drop of n-hexane in distilled water)
- An alcohol burner to evaporate a drop of sample.
- A four-way valve to control the direction of gas flow.
- A 3L air bag to stabilize the concentration of gaseous sample before introduced through the photocatalyst layer.

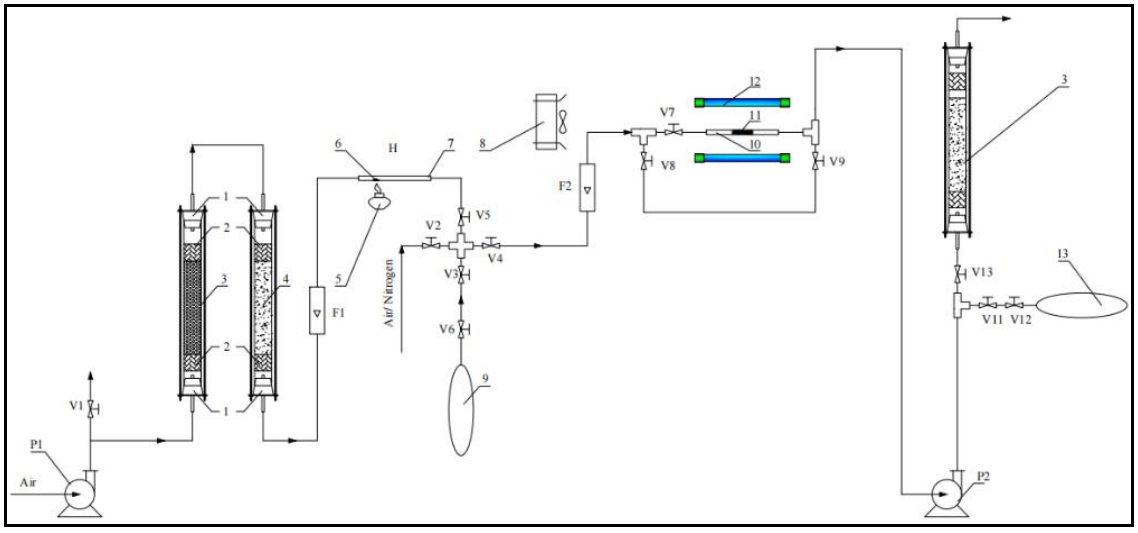

Fig.1: Schematic diagram of n-hexane treatment using Ir-doped TiO_2 photocatalyst system in laboratory.

1. Rubber cap; 2. Glassy cotton; 3. Silicagel; 4. Activated carbon; 5. Alcohol burner; 6. Sample drop; 7. Glassy tube; 8. Cooling fan; 9. Bag containing inlet gas; 10. Reaction tube; 11. Photocatalyst; 12. UV light; 13. Bag containing outlet gas.P1: Pumping air in; P2: Withdrawing air out; F1: Flow meter for inlet gas; F2: Flow meter for gas passing through photocatalyst.

2.4 Treatment process of n-hexane

The tightness of the system was checked by using soap on the joints and using a pump to blow air through the system; if soap bubbles did not present, then the system was utterly sealed. System tightness testing was conducted at the beginning of the test sessions. During the testing sessions, the tightness test would be re-run and corrected whether the following signs were observed: the joint was not sealed, the flowmeters F1 and F2 were not working or working weaker, the tension of the airbag was not adequate after a certain period of air collection.

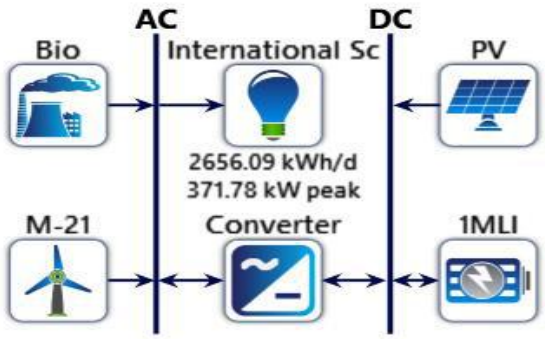

Experiment according to the following steps: (i) Fasten the inlet sample airbag to the connection position with valve V3, open valve V6 (airbag valve), set flowmeter F1 to 1 liter/min, lock all valves, stuff glass wool, and drops of a sample (consisting of 0.02 mL n-hexane and V mL distilled water) into the sample dropper tube, light the alcohol burner, and heat the glass tube containing the droplet over the flame for 1 min; (ii) Open valve V5 and V3, then turn on pump P1 and start a timer simultaneously, collect air within 3 minutes to fill the bag, turn off valve V6 of the airbag, turn off pump and alcohol burner, lock remaining valves; (iii) Stuff 0.1g of the synthesized catalyst material into the glass tube, divide the amount of catalyst into three equal segments alternating with glass wool samples so that the catalyst is evenly distributed on the tube. Turn on the radiator fan, UV lamp, let the UV lamp works for 10 minutes before operating to ensure that the emitted radiation is stable, fasten the airbag to the connection position with valve V11, open valve V12 of the airbag; (iv) Turn on pump P2, open valve V6, and start pressing the timer simultaneously; collect investigated air for the time t (minutes) with the set flow until the airbag reaches the appropriate tension. Lock valve V12, V11, remove the gas sample's airbag, turn off pump P2, and turn off the UV lamp; (v) After the gas collection is complete, clean the system: glass tubes containing sample drops and catalyst column; lock valve V3, open valve V2, and V13 to blow air into the system, then close all valves. Hence, prepare for the next experiment and (vi) After being labeled with the symbol, the airbag containing the sample is placed in the tank and transferred to the analysis company to conduct gas chromatographic analysis for determining the concentration of n-hexane.

III. RESULTS AND DISCUSSION

3.1 Characterization of It-doped TiO_2 Photocatalyst with different ratio of Ir doping in TiO_2

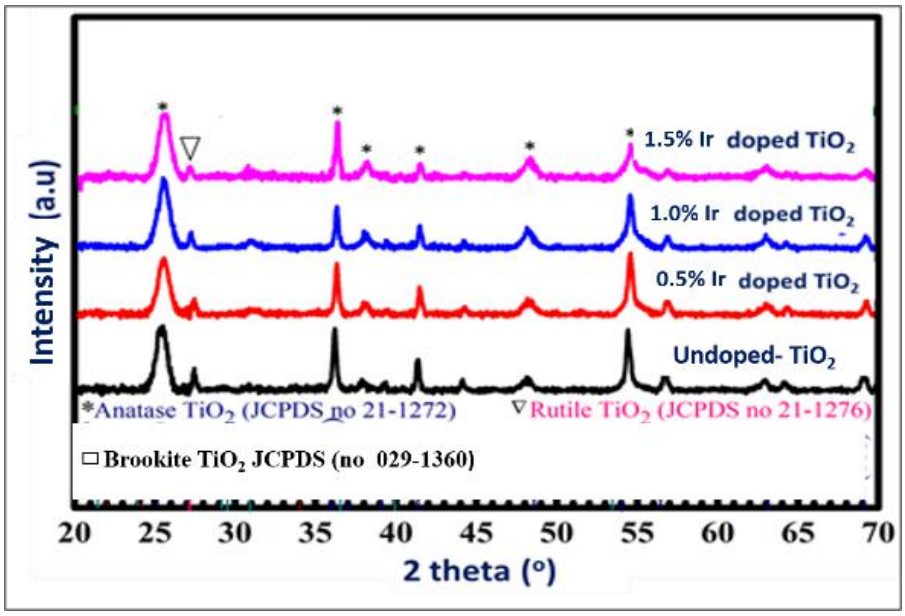

Fig.3: X-ray diffraction patterns of Ir-doped TiO_2 photocatalysts with different Ir-doped ratios of 0.5%, 1.0%, 1.5% respectively

Figure 3 shows XRD measurement of the photocatalysts with different Ir-doped ratios of 0.5%, 1.0%, 1.5%. The result shows the diffraction peaks of pure undoped-TiO_2 are at 2θ positions of $25°, 36°, 41°, 48°, 55°, 57°, 63°, 69°$ respectively corresponding to (101), (103), (210), (200), (105), (201) faces, in which the (204) and (116) faces might relate to anatase TiO_2 phase tetrahedral. The peaks of IrO_2 are not obtained, thus it might show that Iridium was successfully doped into TiO_2 structure. The intensive peaks at 2θ positions of $25°, 36°, 55°$ indicate the crystallographic orientation of anatase phase, besides that, the peak at 2θ position of $27°$ corresponds to the crystallographic orientation of rutile phase. The intensive peaks show that the formation of anatase phase is more preferred than formation of rutile phase.

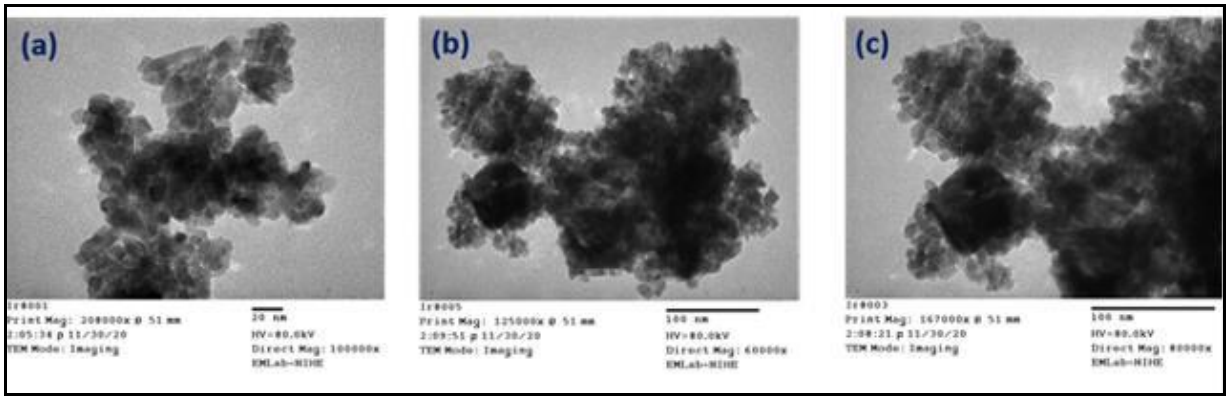

Fig.4: TEM images of Ir-doped TiO_2 photocatalysts with different Ir-doped ratios of (a) 0.5%; (b) 1.0%; (c) 1.5%

The formations of Ir-doped TiO_2 nanoparticle samples shown in Figure 4 indicate that the synthesized photocatalytic material mainly have cubic structure and average size of particles is from 10 to 15 nm. The nanorod particles are corresponding to the formation rutile phase, while the nanocube particles are related to anatase phase. The existence of two particle structures is related to two phases, anatase and rutile. The predominace nanocube particles (anatase phase) is resistent with the XRD result. In addition, the particles are uniformly distributed although the clusters still exist. It is found that from other previously studied M-doped TiO_2 photocatalysts, which are usually synthesized by sol-gel method combined with heat treatment at high temperature ($>500°C$) forming large particles, the Ir-doped TiO_2 photocatalyst is synthesized by hydrothermal method in this work resulting in smaller particles.

Table 1. XRF analysing results of Ir-doped TiO_2 photocatalysts with Ir-doped ratios of 0.5%; 1.0%; 1.5% respectively

No.	Sample	Ir proportion in sample (XRF measurement)
1	0. 5% Ir doped TiO_2	0.62%
2	1.0% Ir doped TiO_2	1.15%
3	1.5% Ir doped TiO_2	1.80%

Table 1 shows the elemental composition of Ti and Ir gives a measure of the doping denaturation ratio by XRF method is close to the calculation theory and at an acceptable level, which shows that the elemental composition of the catalyst can be controlled relatively easily through modification of the initial precursors ($IrCl_3.xH_2O$ và $TiCl_4$). However, the actual ratio tends to be positively error, which can be explained by the fact that $TiCl_4$ is easily hydrolysed when exposed to the external environment, so the loss of TiO_2 may be due to the addition of $TiCl_4$ into the solution. The solution has a small amount of $TiCl_4$ hydrolyzed.

The surface area of the synthesized catalyst samples was analyzed by N_2 adsorption and desorption with Ir-doped TiO_2 catalyst samples, which have the proportions of 0.5%; 1.0%; 1.5% were presented in Table 2.

Table 2. BET analysis results

No	Sample	Specific surface area (m^2/g)	Pore side (nm)
1	0. 5% Ir doped TiO2	156	2,2
2	1.0% Ir doped TiO2	164	2,7
3	1.5% Ir doped TiO2	170	3,1

The surface area of the synthesized catalyst samples was investigated by N_2 adsorption and desorption. The results showed that the Ir-doped TiO2 nano photocatalyst material at the proportion of 1.5% Iridium had the highest specific surface area of 170 m^2/g. This outcome was consistent with the TEM analysis results because the small cubic particle size makes the material's specific surface area higher.

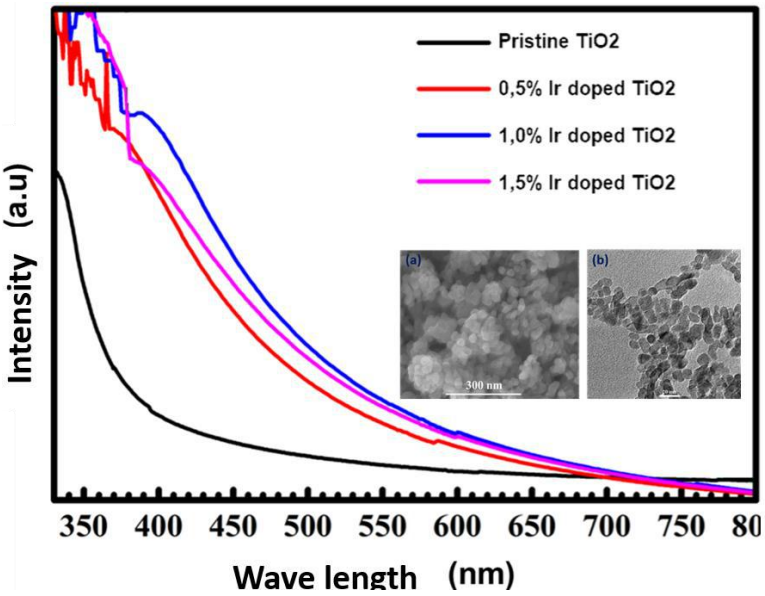

Fig.6. UV-VIS analysis results of 0.5%, 1.0% and 1.5% Ir-doped TiO2 catalyst

In Figure 6, a significant difference could be observed in the absorption of the undoped TiO_2 and Ir-doped TiO_2 photocatalysts having different Ir concentrations. In the wavelength region less than 400 nm, absorption of undoped TiO_2 was observed because its bandgap was related to the bandgap excitation of anatase TiO_2 corresponding to this region-to-region transition. On the other hand, the Ir-doped TiO_2 samples having different Ir concentrations showed an apparent absorption in the longer wavelength region, and the bandgap energy decreased from 3.2 (eV) to 2,5 (eV) in the visible irradiation

3.2 The efficiencty of n-hexane treatment by Ir-doped TiO_2 photocatalyst with different Ir-doped ratio of 0.5%; 1.0%; 1.5%

3.2.1 Effect of Ir-doped ratios on n-hexane decomposing efficiency

Table 3. The experimental parameters in analysing the effect of Ir-doped ratios to n-hexane decomposing efficiency

No	**Iridium proportion** *(%)*	**n-hexan volume** *(mL)*	**H_2O volume** *(mL)*	**Measure humidity** *(%)*	**Airflow rate** *(mL/min)*	**Time for obtaining gas** *(min)*
1	0.5	0.02	0.11	72	200	15.80
2	1.0				200	15.28
3	1.5				200	15.23

Table 4. Gas chromatography results of determining n-hexane concentrations, corresponding with 0.5%; 1.0%; 1.5% Ir-doped TiO_2 samples

No	Iridium proportion (%)	Concentrations of n-hexan before reactions C_o (mg/m^3)	Concentrations of n-hexan after reactions C_m (mg/m^3)	Decomposing efficiency H (%)
1	0.5	10591	4534	57.18
2	1.0		4616	56.42
3	1.5		4799	54.68

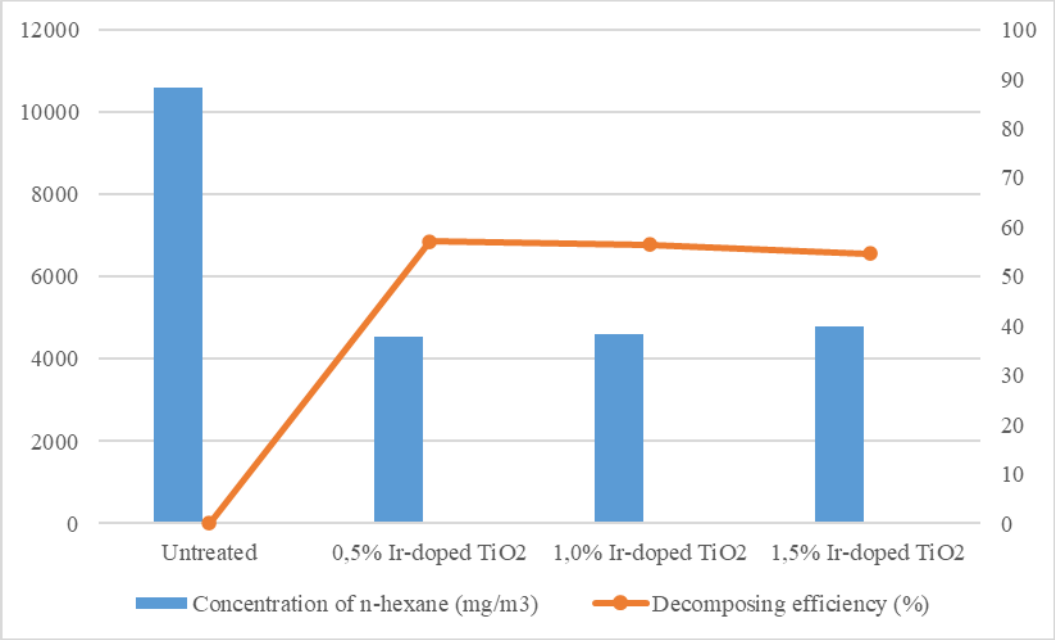

Fig.7. Effect of Ir-doped ratios on n-hexane decomposing efficiency

Table 3 shows the experimental parameters in analysing the effect of Ir-doped ratios to n-hexane decomposing efficiency. Table 4 and the Figure 7 show the concentrations of n-hexane in gaseous sample before and after being treated with Ir-doped TiO_2 photocatalyst with different Ir-doped ratios. The reactions are taken place with the conditions of n-hexane and H_2O sample drops of 0.02mL and 0.11mL respectively (corresponding with the measured humidity of 72%), the 200mL/min airflow rate and 15min residence time to fulfill TEDLAR BAG 3L airbag. After finishing the experiments, with gas chromatography analysis, the n-hexane concentrations in 0.5%; 1.0%; 1.5% Ir-doped TiO_2 are 4534 4534 (mg/m^3), 4616 (mg/m^3) and 4799 (mg/m^3) respectively and the corresponding decomposing efficiencies are 57.18%, 56.42%, 54.68% respectively and the difference is not large. This result indicates that the Iridium proportion has negligible effect on n-hexane decomposing efficiency. For a saturated hydrocarbon and hardly decomposed compound like n-hexane, the obtained efficiencies of more than 50% are relatively

high. Different from treating, for the n-hexane, 0.5% Ir-doped TiO_2 sample has the higher decomposing efficiency than that of other samples (57.18%), therefore it is chosen to be the optimizing efficiency for the following analyses

3.2.2 Effect of airflow rate on n-hexane decomposing efficiency

Table 5: The experimental parameters in analysing the effect of airflow rate to n-hexane decomposing efficiency

No.	**Ir proportion** *(%)*	**Volume of n-hexan drop** *(mL)*	**Volume of H_2O drop** *(mL)*	**Measured humidity** *(%)*	**Airflow rate** *(mL/min)*	**Residence time** *(phút)*
1	0,5	0,02	0,11	72	125	24,12
2					200	15,28
3					350	8,75

Table 6: Gas chromatography results of determining n-hexane concentrations, corresponding with airflow rate of 125,200,350 (mL/min) respectively

No.	**Airflow rate** *G (mL/min)*	**n-hexane concentration before reactions** *C_o (mg/m^3)*	**n-hexane concentration after reactions** *C_m (mg/m^3)*	**Efficiency** *H (%)*
1	125	10591	4529	57.24
2	200		4534	57.18
3	350		4585	56.71

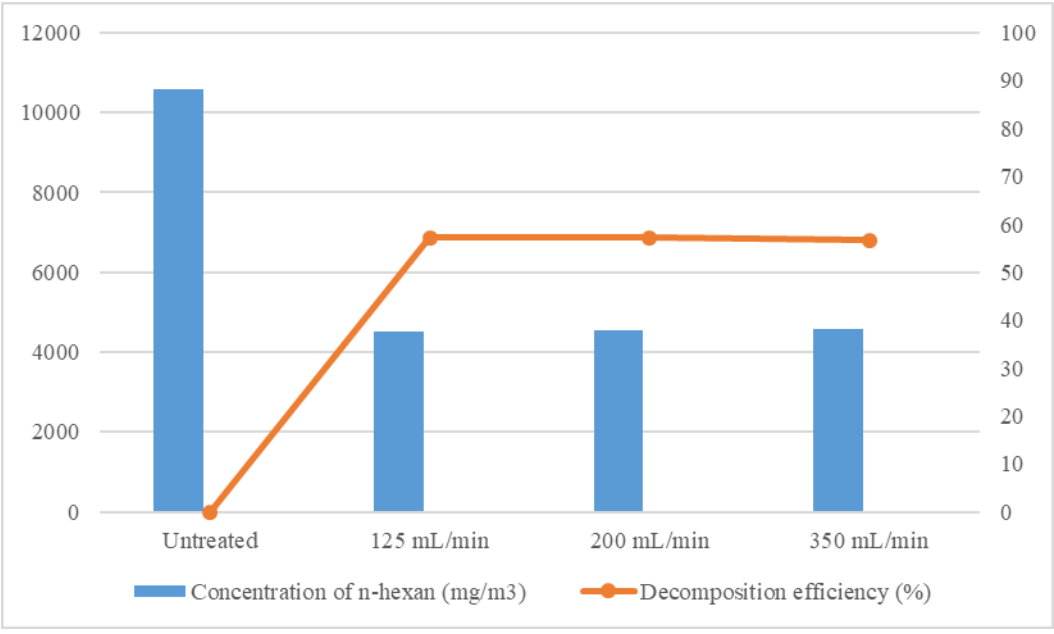

Fig. 8. Effect of airflow rate to n-hexane decomposing efficiency

Table 5 shows the experimental parameters in analysing the effect of Ir-doped ratios to n-hexane decomposing efficiency. Table 6 and the Figure 8 show the concentrations of n-hexane in gaseous sample before and after being treated with Ir-doped TiO_2 photocatalyst with different airflow rate of n-hexane. The results chromatographic analysis determined that the concentration of n-hexane was 4529 mg/m3; 4534 mg/m3; 4585 mg/m^3, from which the corresponding efficiency is 57.24%; 57.18%, and 56.71%. Besides, the selection of optimal conditions needs to combine the factors of time, resources and economy, so in this case, the loading rate is 350 mL/min (the gas collection time is 8, 5 min) is the optimal condition for n-hexane treatment.

3.3 Proposed Mechanism of n-hexane decomposing reaction of Ir-doped TiO_2 photocatalyst

The n-hexane decomposition efficiency of Ir doped-TiO2 materials was compared with previous studies as shown in Table 7. Compared with these results, these results are higher than previous studies on the n-hexane processing ability of Ir-doped TiO_2, showing that the n-hexane processing efficiency of Ir-doped TiO2 with different ratios gives the same efficiency. The higher processing efficiency than other studies was explained by the optimal Ir-doped TiO2 synthesis toward 10-15 nm nano-sized materials, large specific surface area, good crystalline structure, and miscibility of the anatase and rutile phases. Especially when denaturing TiO2 by Ir, the bandgap of Ir-doped TiO_2, depending on the denaturation ratio, decreased to 2.4-2.7 eV compared to 3.2eV of undoped TiO_2. The ionic role of the Ir metal affected the photoreactivity of TiO_2 catalyst by using an electron or hole "trapping" mechanism, thereby changing the recombination rate of e-/h+ (electrons/holes) despite the low bandgap of Ir-doped TiO2 photocatalysts. The above results show that the new Ir -doped TiO2 nanoscale photocatalyst material was a potential catalyst and could be widely applied to treat n-hexane.

Table 7: Results in analysing Ir-doped TiO_2 photocatalyst for n-hexane decomposing

STT	VOCs	Nanomater-ials	Synthetic method	Morphology	Conditions	Efficiency	Refs
1	n-Hexan	TiO_2 on carbon tubes	Method of covering on supporter	The size is about 3.1 nm. Large specific surface area (887.7 m^2/g)	Concentration of n-hexan: 500 ppb, relative humidity : 40-60%	50%	[28]
2	n-Hexan	TiO_2 on glass fibers	Method of covering on supporter	The size is 3,5 nm	n-hexan concentration: 500 ppb, relative humidity : 40-60%	25%	[28]
3	n-Hexan	Ir-doped TiO_2	hydrothermal	The size is about 10-15 nm	Concentration of n-hexan : 10590 ppm	57%	In this study

The mechanism of treating toxic compound n-hexane in the air using Ir-doped TiO_2 photocatalyst was proposed as follows:

Electron separation process:

Electron and hole pairs would be produced whenever the sample material was irradiated with an appropriate light source. These electrons and holes would be the main oxidizing agents, but they moved freely in the lattice and easily recombined with each other:

Ir-(TiO_2) $e_{cb}^- + h_{vb}^+$

Electron trap process:

In making Ir-doped TiO_2 materials, Ir3+ ions were converted into Ir^{4+} and replaced in positions of Ti4+ ions in the crystal lattice, causing defects in the lattice. From the obtained results, based on the electron trapping and displacement mechanism proposed by Choi et al., the role of Ir in the Ir-doped TiO_2 crystal lattice was described as follows:

Electrons trap center: $Ir^{4+} + e_{cb}^- \rightarrow Ir^{3+}$ (4.2)

Holes trap center: $Ir^{4+} + h_{vb}^+ \rightarrow Ir^{5+}$ (4.3)

Electron Transfer Reaction

After trapping the electron pairs, Ir metal would transfer electrons to the redox participating agents O2 and OH-:

$Ir^{5+} + OH^- \rightarrow OH\cdot$ (4.4)

$Ir^{3+} + O_2 \rightarrow O_2^{\bullet-}$ (4.5)

Due to the ability to trap both electrons and holes, the treatment efficiency of Ir-doped TiO2 catalyst was higher than other M-doped TiO2 catalysts. If only one of the two were trapped, the reaction efficiency would be low because the charges dissociate from the trap and move to the phase interface. The trap mechanism helped prevent the recombination of electrons and holes, increasing the lifetime of photogenerated electrons, thereby improving catalytic efficiency [27]. The water molecule adsorbed on the catalyst reacts with the hole, produces a hydroxyl radical, and oxidizes the organic compound. Photochemical reactions have been shown to depend on the production of hydroxy molecules [29], [30]. Oxygen is essential for photochemical reactions to occur. Usually, the rate of organic matter decomposition increases with oxygen concentration [31].

The treatment mechanism for organic compounds such as n-hexane by Iridium modified TiO2 photocatalyst could be summarized in Figure 9.

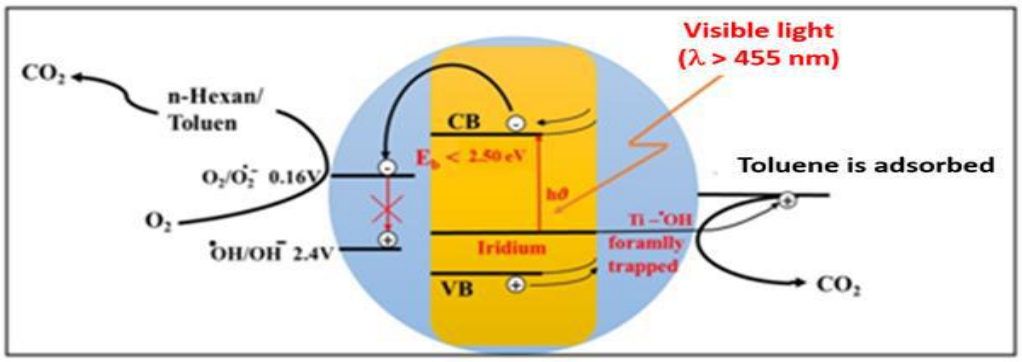

Fig.9. A proposed mechanism to degrade toxic organic compounds using Ir-doped TiO2 nano-sized photocatalyst materials.

IV. CONCLUSIONS

In this research, we have synthesized and analyzed the properties of TiO_2 photocatalyst materials modified at the low Ir concentration with different Ir doping concentration (0.5%, 1%, and 1.5%). We found that the Iridium-doped TiO_2 photocatalyst materials, which were formed by higher anatase phase at different Ir concentrations, had a cubic-shaped particle with an average size in the range of 10 to 15 nm; the 1.5% Iridium sample had reached the specific surface of 170 m2/g, and its lowest energy bandgap was 2.5 eV. The n-hexane toxic volatile organic compound treatment system was instated to evaluate the ability of decomposing n-hexane at different Ir concentrations and different n-hexane gas flows. Interestingly, it was fond that the decomposition efficiency by Ir doped-TiO_2 reached to 57% for n-hexane decomposition, which caould be explained by the ion of the modified metal Ir reducing the bandgap to 2.5 - 2.7 eV. It affected the photo-reactivity of TiO_2 by acting as an electron/hole "trap," thereby changing the rate of e-/h+ recombination (electron/ holes) toward improving the n-hexane decomposition efficiency. The above results showed that the new nanoscale photocatalyst material TiO_2 modified Iridium was a potential catalyst and could be widely applied in treating toxic VOCs such as toluene, benzene, acetone.

ACKNOWLEDGMENTS

This work is supported by Project of Ho Chi Minh City of Department of Science and Technology (DOST)-2019/HĐ-QPTKHCN. Thanks to Mr. Pham Minh Toan, Mr. Pham Quoc Hau and Dr. Huynh Thien Tai for your supports for this work.

REFERENCES

[1] Zhong, L., et al., *Modeling and physical interpretation of photocatalytic oxidation efficiency in indoor air applications.* Building and Environment, 2010. **45**(12): p. 2689-2697.

[2] Zhao, J. and X. Yang, Photocatalytic *oxidation for indoor air purification: a literature review.* Building and Environment, 2003. **38**(5): p. 645-654.

[3] Jo, S.-H., et al., *Deodorization of food-related nuisances from a refrigerator: The feasibility test of photocatalytic system.* Chemical Engineering Journal, 2015. **277**: p. 260-268.

[4] Zhong, L., et al., *Performance of ultraviolet photocatalytic oxidation for indoor air applications: systematic experimental evaluation.* Journal of hazardous materials, 2013. **261**: p. 130-138.

[5] Dong, H., et al., *An overview on limitations of TiO_2-based particles for photocatalytic degradation of organic pollutants and the corresponding countermeasures.* Water Res, 2015. **79**: p. 128-46.

[6] Chen, X. and S.S. Mao, *Titanium dioxide nanomaterials: synthesis, properties, modifications, and applications.* Chemical reviews, 2007. **107**(7): p. 2891-2959.

[7] Yuan, R., et al., *Enhanced photocatalytic degradation of humic acids using Al and Fe co-doped TiO_2 nanotubes under UV/ozonation for drinking water purification.* Journal of hazardous materials, 2013. **262**: p. 527-538.

[8] Yuan, R., B. Zhou, and L. Ma, *Removal of toluene from water by photocatalytic oxidation with activated carbon supported Fe^{3+}-doped TiO_2 nanotubes.* Water Science and Technology, 2014. **70**(4): p. 642-648.

[9] Shayegan, Z., C.-S. Lee, and F. Haghighat, *TiO_2 photocatalyst for removal of volatile organic compounds in gas phase – A review.* Chemical Engineering Journal, 2018. **334**: p. 2408-2439.

[10] Houšková, V., et al., *Efficient gas phase photodecomposition of acetone by Ru-doped Titania.* Applied Catalysis B: Environmental, 2009. **89**(3-4): p. 613-619.

[11] Tseng, H.-H., et al., *Degradation of xylene vapor over Ni-doped TiO_2 photocatalysts prepared by polyol-mediated*

synthesis. Chemical Engineering Journal, 2009. **150**(1): p. 160-167.

[12] Jin, M., et al., *Photochromism-based detection of volatile organic compounds by W-doped TiO_2 nanofibers.* J Colloid Interface Sci, 2011. **362**(1): p. 188-93.

[13] Hinojosa-Reyes, M., et al., *Gas-phase photocatalytic decomposition of ethylbenzene over perlite granules coated with indium doped TiO_2.* Chemical Engineering Journal, 2013. **224**: p. 106-113.

[14] Inturi, S.N.R., et al., *Visible-light-induced photodegradation of gas phase acetonitrile using aerosol-made transition metal (V, Cr, Fe, Co, Mn, Mo, Ni, Cu, Y, Ce, and Zr) doped TiO_2.* Applied Catalysis B: Environmental, 2014. **144**: p. 333-342.

[15] Huang, H., et al., *Enhanced degradation of gaseous benzene under vacuum ultraviolet (VUV) irradiation over TiO_2 modified by transition metals.* Chemical Engineering Journal, 2015. **259**: p. 534-541.

[16] Sun, S., et al., *Photocatalytic degradation of gaseous toluene on Fe-TiO_2 under visible light irradiation: A study on the structure, activity and deactivation mechanism.* Applied Surface Science, 2012. **258**(12): p. 5031-5037.

[17] Oseghe, E.O., P.G. Ndungu, and S.B. Jonnalagadda, *Photocatalytic degradation of 4-chloro-2-methylphenoxyacetic acid using W-doped TiO2.* Journal of Photochemistry and Photobiology A: Chemistry, 2015. **312**: p. 96-106.

[18] Li, F.B., et al., *Enhanced photocatalytic degradation of VOCs using Ln^{3+}-TiO_2 catalysts for indoor air purification.* Chemosphere, 2005. **59**(6): p. 787-800.

[19] Chen, X. and C. Burda, *The Electronic Origin of the Visible-Light Absorption Properties of C-, N- and S-Doped TiO_2 Nanomaterials.* Journal of the American Chemical Society, 2008. **130**(15): p. 5018-5019.

[20] Liu, G., et al., *Visible Light Responsive Nitrogen Doped Anatase TiO_2 Sheets with Dominant {001} Facets Derived from TiN.* Journal of the American Chemical Society, 2009. **131**(36): p. 12868-12869.

[21] Dhanalakshmi, M., et al., *Fabrication of novel surface plasmon resonance induced visible light driven iridium decorated SnO_2 nanorods for degradation of organic contaminants.* Journal of Alloys and Compounds, 2018. **763**: p. 512-524.

[22] Menéndez-Flores, V.M. and T. Ohno, *High visible-light active Ir-doped-TiO_2 brookite photocatalyst synthesized by hydrothermal microwave-assisted process.* Catalysis Today, 2014. **230**: p. 214-220.

[23] Pawluk, T., Y. Hirata, and L. Wang, *Studies of Iridium Nanoparticles Using Density Functional Theory Calculations.* The Journal of Physical Chemistry B, 2005. **109**(44): p. 20817-20823.

[24] Rojas, J.V. and C.H. Castano, *Radiolytic synthesis of iridium nanoparticles onto carbon nanotubes.* Journal of Nanoparticle Research, 2014. **16**(8).

[25] L. Atanasoska, P.G., C. Denga, R. Warnera, S. Larsen, J. Thomson, *XPS, AES, and Electrochemical Study of Iridium Oxide Coating Materials for Cardiovascular Stent Application* ECS Transactions, , 2009. **16** p. 37-48.

[26] Shannon, R.D., *Revised effective ionic radii and systematic studies of interatomic distances in halides and chalcogenides.* Acta crystallographica section A: crystal physics, diffraction, theoretical and general crystallography, 1976. **32**(5): p. 751-767.

[27] Choi, et al.(2002), The role of metal ion dopants in quantum-sized TiO_2: Correlation between photoreactivity and charge carrier recombination dynamics. *The Journal of Physical Chemistry*, 98(51), 13669-13679.

[28] Zahra, et al.(2018), TiO_2 photocatalyst for removal of volatile organic compounds in gas phase – A review. *Chemical Engineering Journal*, *334, 2408–2439*

[29] Park, et al. (1999). Photocatalytic oxidation of ethylene to CO_2 and H_2O on ultrafifine powdered TiO_2 photocatalysts in the presence of O_2 and H_2O. *Journal of Catalysis 185, 114–119.*

[30] Tompkins, et al. (2001). Evaluation of photocatalytic air cleaning capability: a literature review and engineering analysis. *ASHARE Research Project RP-1134*.

[31] Chang, et al. (2003), *Heterogeneous photocatalytic oxidation of acetone for air purification by near UV-irradiated titanium dioxide*, Journal of Environmental Science and Health Part A – Toxic/Hazardous Substances & Environmental Engineering 38, 1131–1143.